Macian Martinez, V.; Tormos, B.; Bermúdez, V.; Bastidas-Moncayo, KS. (2021). Development of a floating liner test rig and lubrication model for the study of the piston compression ring friction force under fully flooded and starved lubrication. Tribology International. 160:1-14. https://doi.org/10.1016/j.triboint.2021.107034

Development of a floating liner test rig and lubrication model for the study of the piston compression ring friction force under fully flooded and starved lubrication

Vicente Macián[a], Bernardo Tormos[a], Vicente Bermúdez[a] and Sophia Bastidas[a,*]

[a]CMT-Motores Térmicos, Universitat Politècnica de València. Camino de Vera S/N, 46022. Valencia, Spain.

ARTICLE INFO

Keywords:
Floating liner
Friction force measurement
Numerical model
parameters tests
Lubricant oil

ABSTRACT

Advances in internal combustion engines make it necessary to study in depth their contribution to engine efficiency, and thus to friction mechanical losses, especially those generated in the piston-cylinder liner assembly. In this paper, the design of a novel test rig is presented, based on the floating liner principle, with the key objective of having the capability of developing multiple parameters tests in a relatively quick and easy way. The final design integrates a single-cylinder internal combustion engine, a mechanical solution that allows the liner to float, three piezoelectric force sensors and a novel design of lateral support based on ball transfer units. Reproducibility and repeatability of tests were assessed demonstrating the capability of the test rig to develop reliable friction measurements. Some parameters tests were developed to evaluate the sensitivity of the friction force measurements to variations in the working conditions, oil temperature and engine speed. A theoretical model for the piston compression ring is presented for both fully flooded and starved lubrication conditions, including asperity interactions and lubricant rheology. Comparisons of these approaches with experimental results showed that, for the working conditions of the test rig, lubrication of the compression ring is better estimated under fully flooded lubrication condition, as the starved lubrication analysis results in over-estimated friction force values at higher engine speed regimes.

1. Nomenclature

A = ring contact area
A_{asp} = asperity area
a, b and c = oil constants
b = circumferential length of the ring
D = bore
E = combined modulus of elasticity
f = friction force
f_b = boundary friction force
F_t = tangential force
f_v = viscous friction force
F_z = load carrying capacity of the oil per unit width
h = oil film thickness
h_{in} = oil film thickness at the liner
h_{left} = oil film thickness left by the ring
h_m = film thickness at $dp/dx = 0$
h_o= minimum oil film thickness
h_s = piston ring profile
i = nodes in the axial direction
j = crank angle iteration
l = compression ring axial height
L = connecting rod length

*Corresponding author
kabasmon@mot.upv.es (S. Bastidas)
ORCID(s):

n = number of nodes on the compression ring axial profile
m = iteration
p = oil pressure
P_c = contact pressure
q_{in} = oil flow rate available to the ring
q_m = oil flow rate at $\partial p/\partial x = 0$
R = crank radius
R_{f1} = compression ring profile radius of curvature
T_0 = oil temperature
t = time
U = velocity of the moving surface in the axial direction, piston speed
V_d = engine displaced volume
W = ring tension force
W_t = total contact reaction
x = axial coordinate of the ring height
x_1 = oil film inlet position
x_1' = oil film inlet position under starvation conditions
x_2 = point where the oil film ruptures
x_3 = oil film reformation point
x_4 = oil film outlet position
y = circumferential coordinate
z = radial coordinate
$\hat{z}$ = fraction of the radial clearance space filled with oil

Non-dimensional terms:
H = oil film thickness = h/h_o
H_m = oil film thickness at $dP/dX = 0$, $H_m = h_m/h_o$
P = oil pressure = $ph_o^2/\eta U l$
Q_{in} = oil flow rate available to the ring at a specific crank angle = h_{in}/h_o
Q_m = oil flow rate at $\partial P/\partial X = 0$, $Q_m = H_m/2$
X = axial coordinate of the ring height = x/l

Greek:
α = crankangle
β = asperity radius of curvature
ϵ_P = tolerance for pressure convergence
ϵ_Q = tolerance for oil flow rate convergence
ϵ_W = tolerance for load convergence
ζ = coefficient of asperity shear strength
η = dynamic viscosity of the oil
θ = crank angle
ρ = asperity density
σ = combined surface roughness
τ = shear stress
ω = angular velocity

2. Introduction

The study of friction in internal combustion engines (ICE), specifically in the piston-cylinder liner assembly has been of great importance for researchers and manufacturers due to its contribution to the engine mechanical friction losses [42, 38, 17, 15], and therefore to the engine efficiency. Improvements in the design of engine components, materials and surface finishes [48, 14, 36, 40, 44, 11, 6, 24, 49], by instance, make it necessary to keep on studying this

phenomenon in depth. For this purpose, floating liner test rigs have been developed by different authors to evaluate the friction force in the piston-cylinder liner interface, as it allows a direct measurement of friction under different working conditions and for multiple parameters tests. The measuring principle of a floating liner consists of isolating the liner from the engine block and suspend it, in such a way that the liner moves freely in the axial direction. Friction force, exerted by the piston over the liner, is therefore only captured by force sensors [31, 37].

Furuhama et al [8] developed the first floating liner test rig using piezoelectric force sensors and with the capability of running tests under fired conditions. Their design has been improved by multiple authors and it has served as baseline for similar research works [46, 19, 27, 20]. Recent studies have also employed this floating liner design without the cylinder head and under motored conditions by means of an electric motor[23, 47, 24]. In order to simulate compressed cylinder conditions, but without having combustion, Law et al [22] developed a test rig with a compressed air injection system, used also to compensate mass losses due to blow-by and leakage through the combustion chamber sealing. This sealing was made by means of a labyrinth seal located at the top of the liner, leaving a gap to avoid any interference with the axial movement of the liner. Results with the test rig showed however, that under compressed conditions, the sealing device was interfering with the liner, causing erroneous friction measurements. Islam [16] continued the work in the test rig, replacing the labyrinth seal with a piston compression ring. With this modification, peak pressures of up to 80 bar were reached during tests, similar to that found during normal engine combustion. Söderfjäll et al [39] on the other hand, designed a simplified floating liner for Heavy-duty diesel (HDD) engines application under ambient pressure conditions.

Regarding the design of this type of test rigs, many difficulties arise during the process, starting from the mechanical solution given to isolate the liner, which in turn implies the selection of force sensors and their location, as they will be the only attachment between the liner and the engine block. One of the main concerns is the sealing of the combustion chamber, so the in-cylinder pressure does not affect the friction force measurement. Multiple solutions have been proposed to balance the in-cylinder pressure by means of modifications to the liner and even to the piston [7, 45, 13, 19, 21]. The floating liner developed by Gore et al [10] employs a labyrinth seal to prevent leakage from the combustion chamber; however, corrections to the measured friction force were needed, given that some pressure leakage was found to act at the top rim of the liner. The lateral force exerted by the piston over the liner is another design parameter to take into account. Different solutions have been employed to restrict this force from interfering with the axial friction force measurement, Wakuri et al, [45] used by instance, eight hydrostatic bearings to support the liner, allowing its axial displacement. The floating liner developed by Söderfjäll et al [40] added a liner guide made of PTFE to assure contact only between the piston ring and the cylinder liner. The floating liner developed by O'Rourke et al [32] on the other hand, employed tri-axial force transducers, which hold the clamps that give radial support to the liner, thus being capable of measuring the forces in the three axis.

In order to estimate the lubrication conditions in the piston-cylinder liner assembly, theoretical models have been developed extensively throughout the years, commonly based on the solution of the Reynolds equation. This solution can be addressed by means of analytical or numerical methods. In the same way, theoretical models can have different levels of complexity, including features to represent the real working conditions of the piston assembly. Dowson et al [3] presented a one-dimensional analytical model for the piston compression ring, assuming fully flooded conditions for all the engine strokes. To model the lubrication of a complete ring pack, flow continuity and ring starvation were included in the model; in this way, the lubricant oil available to the inlet of the ring was equal to that left behind by the preceding ring. Hydrodynamic lubrication was assumed and friction force was obtained from the integration of the viscous stress in the regions of fluid film lubrication.

A different approach was applied by Ma et al [25], for the lubrication of one piston ring including starvation and cavitation conditions. It consisted of a switching function or cavitation index that changed according to the region, full film or cavity, where the Reynolds equation was applied. The model took into account the mass conservation principle to estimate the oil available at the inlet of the interface, including the oil accumulation in front of the ring. The model was solved numerically using the finite differences method.

Hydrodynamic lubrication was assumed by D'Agostino et al [1], assuming also that surfaces were smooth, and that oil viscosity and density were constant with temperature. To include the surface topography of the ring and the liner, Morris et al [29] used the approach by Greenwood and Tripp [12], to model the lubrication in one piston ring. The model was based on the work previously developed by Patir and Cheng [34], using the flow factors approach. Friction force was then estimated for both hydrodynamic and boundary lubrication, from the asperity interactions of the surfaces. In a later work by Gore et al [9], an analytical model was presented and compared to results in a floating liner. The model included both boundary and hydrodynamic lubrication, assuming a fully flooded inlet condition for

the ring. Viscosity and density of the lubricant oil varied with the temperature and pressure working conditions.

Up to this point, direct comparisons between experimental measurements of friction losses in the floating liner and simulation results had only been reported in the work by Gore et al [9], and only for fully flooded lubrication conditions, which could not completely represent the actual lubrication of the piston rings. This is specially important for the compression ring, that has been demonstrated to work under starved lubrication for most of the engine cycle [28, 37, 39]. Include fully flooded as well as starved lubrication to the comparison of theoretical and experimental results of the piston compression ring lubrication in a floating liner, represents a gap in the current research work developed on this subject.

In this paper, a new floating liner has been developed with the aim of providing a test rig that allows the study of friction in the piston-cylinder liner assembly in an accurate and easy way. For this purpose, the design of the rig was aimed to facilitate the exchange of engine components for multiple parameters tests, and it is operated under ambient pressure conditions, by means of an electric motor. A theoretical model for the piston compression ring using the finite differences method is also presented, including hydrodynamic and boundary lubrication conditions. Fully flooded condition is initially assumed for the piston compression ring, however, starved lubrication was also included in the model to account for flow continuity. These two assumptions for the piston ring lubrication were then compared with experimental results in the floating liner. The novelty of the research work presented here includes the modular design of the floating liner, that helps with the components exchange, and the solution proposed for the lateral force restriction based on ball transfer units; this design has not been reported in previous literature. Regarding the piston compression ring lubrication model, although it has been widely presented by different authors [26, 29, 33], as well as the study of its friction force contribution trough experimental tests [9, 49], the comparison of friction force results under fully flooded and starved lubrication conditions with experimental data is not easily found in literature, as discussed in the previous paragraph, and therefore it is a main contribution of the work presented here to this subject.

3. Development of the Floating Liner

The measuring principle of a floating liner test rig consists of suspending the cylinder liner in such a way that the small axial displacement of the liner, due to the reciprocating motion of the piston, is restricted only by sensors, which in turn are attached to the test rig structure [32]. The friction force generated between the piston and the liner is then captured by the sensors directly. With this in mind, the design of the floating liner presented here was developed with some key targets. The main one consisted of having the capability to develop different parameters tests with reliable results, which implied a design simple enough to facilitate the assembly and disassemble of the rig, allowing repetitive results. It was also determined that tests would be developed without combustion and under ambient pressure conditions; this with the aim of avoiding measurement inaccuracies due to combustion. Friction force tests under ambient pressure imply significant differences with the actual friction losses experienced by the piston assembly under combustion conditions. Apart from the differences in the order of magnitude of the friction force values, the biggest differences would be expected during the compression and expansion strokes, where the high in-cylinder pressure increases the applied force, specially for the compression ring, causing more severe lubrication conditions. Furthermore, the floating liner without combustion allows to study the direct effect of different parameters over friction without the influence of the combustion chamber pressure variation. Finally, the floating liner design was thought to allow the exchange of components, piston, rings and liner, of different geometric dimensions, with the restriction of a liner external diameter of up to 110 mm.

3.1. Base engine

A single cylinder motorcycle ICE was selected as base for the design of the floating liner; its main characteristics are presented in Table 1. In this air-cooled engine, the liner was incorporated to the engine block as a single unit, making it necessary to replace the whole cylinder block, leaving only the crankcase as baseline for the design of the floating liner.

3.2. Design of the test rig

The floating liner test rig consists of a modular design with different components: a liner with a disc in its external face to attach the three force sensors at 120^{o} spacing; a base plate that serves as joint with the crankcase of the internal combustion engine (ICE), the force sensors are also attached to this component; two cylinders of the same dimensions that make up the external structure of the floating liner, they comprise two rims at the top and bottom to be bolted to

Bore x Stroke	[mm]	105 x 90
Volumentric capacity (displacement)	[cc]	780
Compression ratio	-	9.5
Max. engine torque	[Nm]	58.8 @ 5500 rpm
Max. power	[kW]	39.1 @ 7000 rpm
Lubrication system	-	wet sump

Table 1
Base engine main characteristics

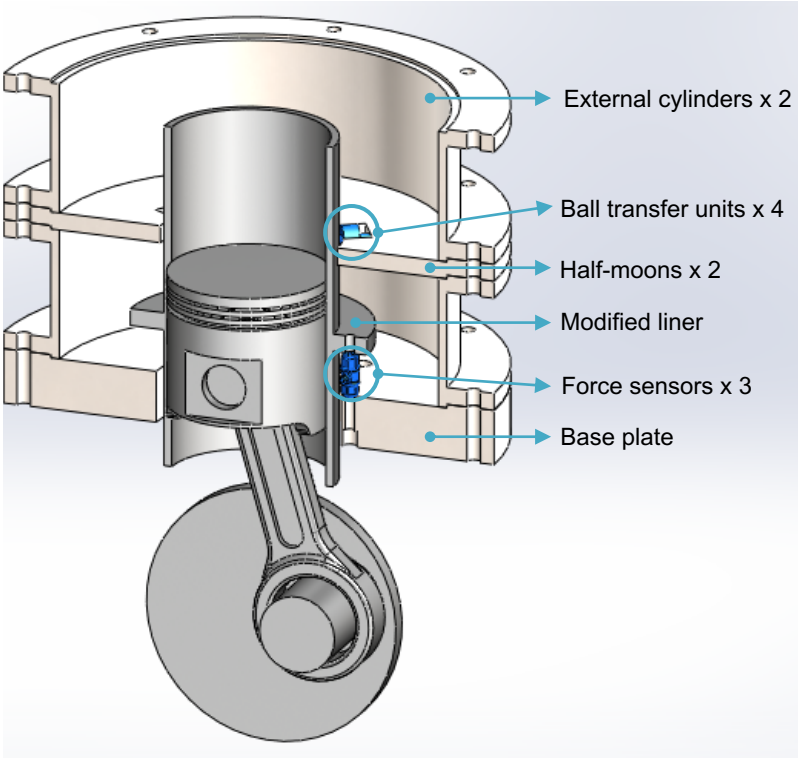

Figure 1: CAD of the floating liner test rig

the rest of the components. Finally, a radial support to restrict the piston lateral force, composed by two half-moons, bolted between the external cylinders, and four ball transfer units. These ball transfer units are omnidirectional bearings consisting of a holding fixture with threaded rod and a ball supported by smaller bearing balls. In this way, the ball transfer units allow the liner to move freely in the axial direction, while restricting the lateral movement of the liner. A CAD of the floating liner test rig is shown in Figure 1, it is a section view of the mechanical components and one of the piezoelectric force sensors. In addition to the objectives mentioned in Section 3, and as a future improvement of the floating liner, a supply of compressed air to the combustion chamber was proposed to better simulate the operation of an ICE. This led to the design of the floating liner with a more robust structure that allows the transmission of the in-cylinder pressure to the rest of the test rig. This explains the use of a thick base plate, of about 30 mm. Under the current working conditions of the floating liner, without in-cylinder pressure, the liner with a wall thickness of 4.5 mm, making it quite rigid, and this component being firmly attached to the force sensors, elastic deformation of the liner is not expected to occur under the operating conditions presented in this study.

For the tests in the floating liner, the procedure followed to assemble/disassemble the ring pack in the floating liner required to remove the external cylinders and the cylinder liner, leaving the piston accessible, but without being removed from the test rig. The rings were removed or installed in the piston using piston ring pliers; while for the cylinder liner assemble, a piston ring compressor set was required, consisting of a metal band of the appropriate

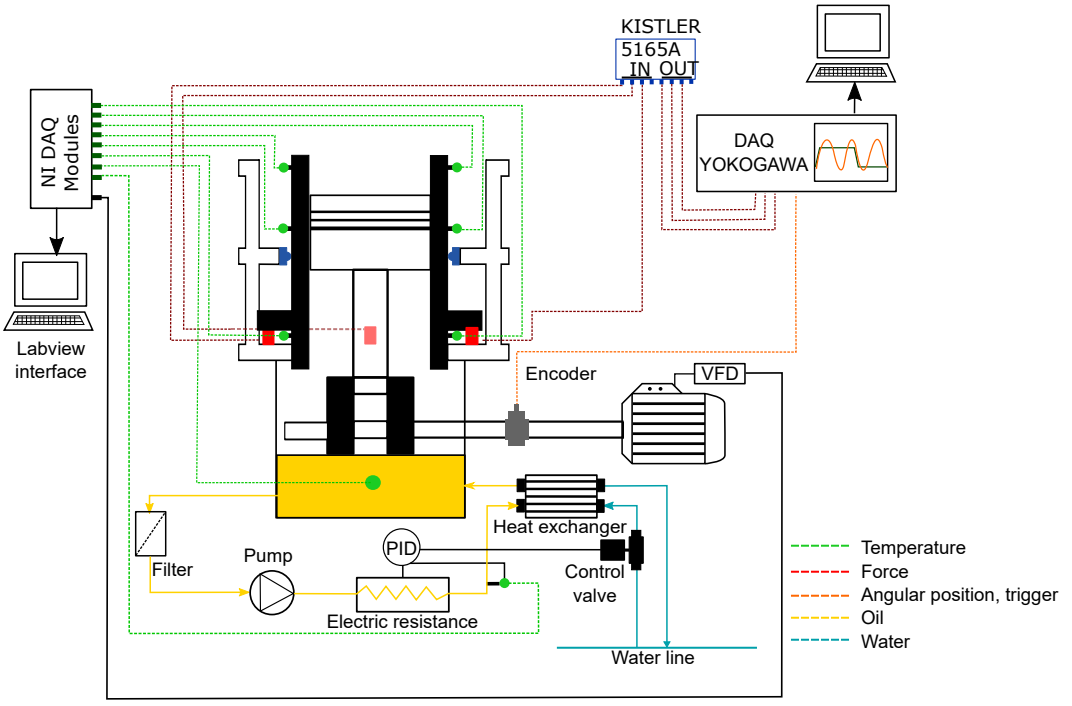

Figure 2: Schematic diagram of the experimental setup

diameter and pliers to secure the band. With the band in place covering the piston and compressing the rings, the liner was installed from its bottom end and slid over the piston to its final position in the test rig.

3.3. Instrumentation

An schematic diagram of the instrumentation of the floating liner is shown in Figure 2. It consists primarily of the three piezoelectric force sensors selected to measure the friction force. These sensors are Kistler quartz force links with a measuring range of $\pm$2.5 kN that have been mounted under preload, therefore they can be used to measure both tensile and compression forces. A hollow shaft encoder was installed in the test rig in order to acquire the crankshaft angular position along with the instantaneous friction force with a resolution of 0.36 degrees. The encoder was employed to trigger the data acquisition of the force sensors. Eight thermocouples type K were located in the test rig, six were installed in the external face of the liner at three different heights and opposed to each other perpendicular to the crankshaft. One thermocouple was located at the bottom of the crankcase to measure the lubricant oil temperature, this reading was employed as reference for the execution of the tests. The last thermocouple was located at the outlet of the electric resistance and was used as feedback to the system that controls the temperature of the oil entering the engine (Section 3.4). Data from the thermocouples was recorded through input modules of a National Instruments data acquisition (NI DAQ) system. For the force sensors, a Kistler 5165A amplifier was used, their analog outputs were transferred to a Yokowaga DAQ system and finally to a computer with the corresponding application software. The encoder measurements were also recorded by this system.

The floating liner operation was integrated in a Labview code to control the electric motor, oil pump and electric resistance. Data from the NI DAQ system was also recorded and displayed through the Labview interface.

3.4. Auxiliary systems

The floating liner test rig comprises two auxiliary systems, shown in Figure 2: the transmission and the lubrication system. The former includes an electric motor with a variable frequency drive (VFD) to adjust the motor speed. Its coupling with the ICE was made with a flexible coupling to absorb any possible misalignment of the shafts. Figure 3 shows the final assembly of this auxiliary system.

Figure 3: Assembly of the transmission system

Test	Engine speed $[rpm]$	Oil temperature $[°C]$	Assembly
1	500	40	1
2	500	40	2
3	2500	40	1
4	2500	40	2
5	500	60	1
6	500	60	2
7	2500	60	1
8	2500	60	2

Table 2
Test points for the performance evaluation of the floating liner test rig

For the floating liner lubrication, an external auxiliary system was mounted with the possibility of controlling the temperature of the oil entering the engine. This system consists of a closed circuit using the own ICE lubrication components; that is, the oil pump, internal oil passages and jets located at the bottom of the liner to lubricate the piston. Regarding the external part of the circuit, it consists of an electric resistance of 6 kW encapsulated in a cylinder full of oil to heat it, an oil pump to return the oil to the crankcase, a heat exchanger and a control valve for the flow of water. The control of the electric resistance and the valve was done through a PID (proportional-integral-derivative controller), the target temperature was compared with the temperature reading of the thermocouple located at the exit of the electric resistance.

4. Performance evaluation of the test rig

In order to test the capability of the floating liner test rig to measure friction with reproducible and repetitive results, tests were proposed with two variables, engine speed and oil temperature. For the reproducibility evaluation, tests were carried out in between two assemblies; that is, one test with the first assembly, followed by a disassemble procedure, and a second test with a new assembly. Each assembly-disassembly task included the upper external cylinder, the two half-moons, and the ball transfer units. Table 2 shows the test points used in this analysis.

The friction force measurements were obtained for an engine cycle of 720^{o}; the comparison between assemblies is presented in terms of the resultant friction mean effective pressure (FMEP) and their percentage difference in Table 3. The FMEP was obtained from equation (1), the instantaneous friction force measurement f, the piston speed U and

Working conditions	FMEP [KPa] Assembly 1	FMEP [KPa] Assembly 2	Difference [%]
40° @ 500 rpm	19.77	19.85	0.42
60° @ 500 rpm	14.86	14.64	1.48
40° @ 2500 rpm	61.61	61.58	0.04
60° @ 2500 rpm	61.91	61.31	0.97

Table 3
Reproducibility results

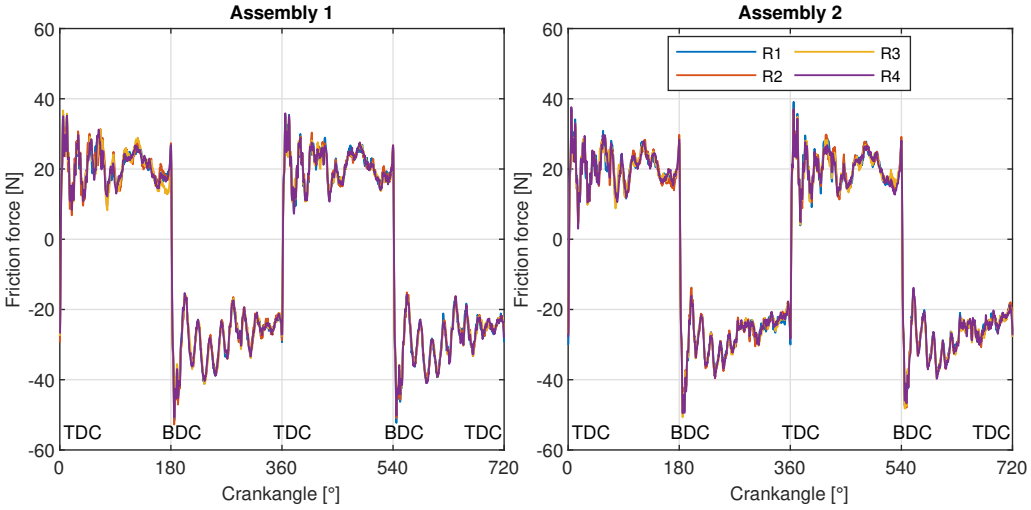

Figure 4: Reproducibility and repeatability tests at 500 rpm and 60°C of oil temperature for the two assemblies

Working conditions	Assembly	Mean FMEP [kPa]	Standard deviation [kPa]	Relative standard deviation [%]
40° @ 500 rpm	1	19.77	0.03	0.13
40° @ 500 rpm	2	19.85	0.04	0.18
60° @ 500 rpm	1	14.86	0.03	0.23
60° @ 500 rpm	2	14.64	0.04	0.30
40° @ 2500 rpm	1	61.61	0.15	0.24
40° @ 2500 rpm	2	61.58	0.13	0.22
60° @ 2500 rpm	1	61.91	0.12	0.20
60° @ 2500 rpm	2	61.31	0.05	0.09

Table 4
Repeatablity results

the engine displaced volume V_d [41].

$$FMEP = \frac{\int fUdt}{V_d} \tag{1}$$

For the cycle-to-cycle repeatability, each test point in Table 2 was measured for a 720º engine cycle and four repetitions. Figure 4 shows the friction force measurements obtained for one set of engine working conditions (500 rpm and oil temperature of 60ºC) and the four repetitions, for the two assemblies in separate plots. The repeatability results are presented in Table 4, including the mean FMEP of the repetitions and the standard and relative deviation of the measurements.

Results of the performance evaluation of the floating liner showed that the test rig allows the measurement of

the instantaneous friction force with a good level of reproducibility and repeatability. The maximum difference in FMEP after an assembly-disassembly task was of about 1.5%. This difference showed to be greater for the higher oil temperature in the two engine speed conditions. The cycle-to-cycle assessment also showed a good response, none of the tested points showed a relative standard deviation higher than 0.30%.

5. Tests definition

Parameters tests in the floating liner were proposed with the aim of evaluating the sensitivity of the test rig to changes in the working conditions of the ICE, and to validate the theoretical model developed for the piston compression ring (Section 6). To accomplish the first objective, tests were developed for five engine speed levels (500, 600, 800, 900 and 1500 rpm) and three oil temperatures (40, 60 and 80°C). For the second purpose, given that the model is for the compression ring, tests were developed with two piston configurations: the configuration A consisting of the complete piston (skirt + ring pack of compression ring, scraper ring and oil control ring), and the configuration B consisting of the complete piston without the compression ring. In this way, the friction force share of the compression ring was obtained as the difference between the measurements of the piston configurations A and B. The main characteristics of the piston and ring pack are included in Table 5.

6. Piston compression ring model

The one-dimensional Reynolds equation, as presented in expression (2), was used to model the lubrication of the piston compression ring. This is a simplified form of the full Reynolds equation with the following assumptions:

$$\frac{\partial}{\partial x}\left(h^3\frac{\partial p}{\partial x}\right) = 6\eta U\frac{\partial h}{\partial x} + 12\eta\frac{\partial h}{\partial t} \tag{2}$$

- The lubricant is Newtonian, therefore the stress is proportional to the shear rate.
- The oil viscosity is constant throughout the film thickness, but varies with the oil temperature.
- There is no side leakage of oil, thus the analysis is kept in one dimension, along the ring axial height.
- The density of the oil is constant with pressure.
- Inertia effects are negligible.

The boundary conditions applied to solve the Reynolds equation, including the Reynolds cavitation condition, are the following:

- Inlet: $p =$ ambient gauge pressure at $x = x_1$
- Cavitation: $p = 0; dp/dx = 0$ at $x = x_2$
- Outlet $p =$ ambient gauge pressure at $x = x_4$

A diagram of the lubrication conditions of the piston compression ring is shown in Figure 5. Given that the floating liner is operated under ambient pressure conditions, the force applied to the ring only comes from the ring tension force W, opposed to the load carrying capacity of the oil film F_z and the force due to the asperity contact F_{asp}. It can also be assumed that the ring inlet is fully flooded with oil; however, experimental research [28, 37, 39] has shown that the piston compression ring normally works under starved lubrication conditions, shown in a dotted line in Figure 5, during most of the engine cycle. In a piston ring pack, starved lubrication is a consequence of the small quantity of oil left by the preceding rings to lubricate the compression ring; in this way, the oil film thickness available in the liner is not enough to fill the ring at $x = x_1$, and the oil inlet moves inwards to $x = x_1'$.

In the cavitation region, the oil pressure falls to a constant value, assumed to be equal to ambient pressure. In this region, the lubricant oil liberates some of the dissolved air in the form of bubbles, and the oil crosses this region in the form of thin streams [4]. This assumption has been adopted by different authors [25, 35, 2], and was also applied in this model for the friction force calculation.

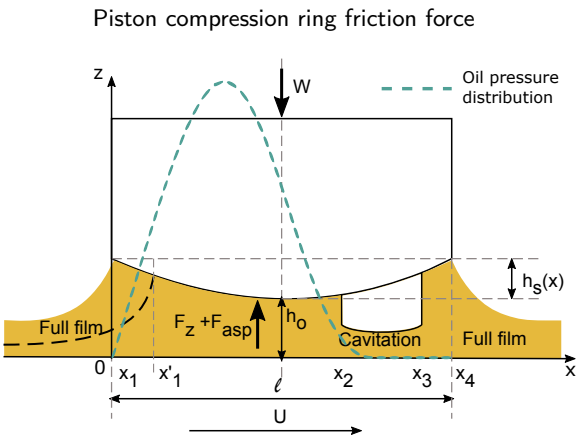

Figure 5: Piston ring lubrication

Piston bore	-	91.42 mm
Piston length	-	86.27 mm
Piston-liner clearance	-	0.220 mm
Compression ring (rectangular) axial height	l	2 mm
Scraper ring (taper faced) axial height	-	2 mm
Oil control ring (DSF) axial height	-	3 mm
Combined modulus of elasticity	E	1.08×10^{11} Pa
Coefficient of asperity shear strength	ζ	0.1
Pressure tolerance	ϵ_P	5×10^{-5}
Load tolerance	ϵ_W	1×10^{-3}
Flow rate tolerance	ϵ_Q	1.5×10^{-2}
Number of nodes on the compression ring axial profile	n	200
Compression ring radius of curvature	R_{f1}	30 mm
$\sigma\beta\rho$	[-]	0.187
Compression ring tangential force	Ft	17.3 N
Lubricant oil	-	SAE 5W30
Oil dynamic viscosity at 40°C	-	56.20 mPa.s
Oil dynamic viscosity at 60°C	-	26.70 mPa.s
Oil dynamic viscosity at 80°C	-	14.62 mPa.s

Table 5
Data used in the experimental tests and for the piston compression ring lubrication model. *DSF: double-bevelled spiral expander ring

The lubrication model described here was developed in the mathematical software Matlab, the flow diagram for its implementation is shown in Figure 6. Furthermore, Table 5 summarizes the geometric dimensions and coefficients used in the model.

To solve the Reynolds equation (2), it was expressed using the following non-dimensional terms:

$$H = \frac{h}{h_o} \qquad X = \frac{x}{l} \qquad P = \frac{ph_o^2}{\eta U l} \qquad t = \frac{\alpha}{\omega} \qquad K_t = \frac{l\omega}{U}$$

Where K_t is a term defined to replace the time step in the last term of equation (2) by an angular position step. h is the oil film defined by the minimum oil film thickness h_o and the piston ring profile h_s, which can be expressed as a parabola:

$$h = h_o + h_s = h_o + \frac{x^2}{2R_{f1}} \tag{3}$$

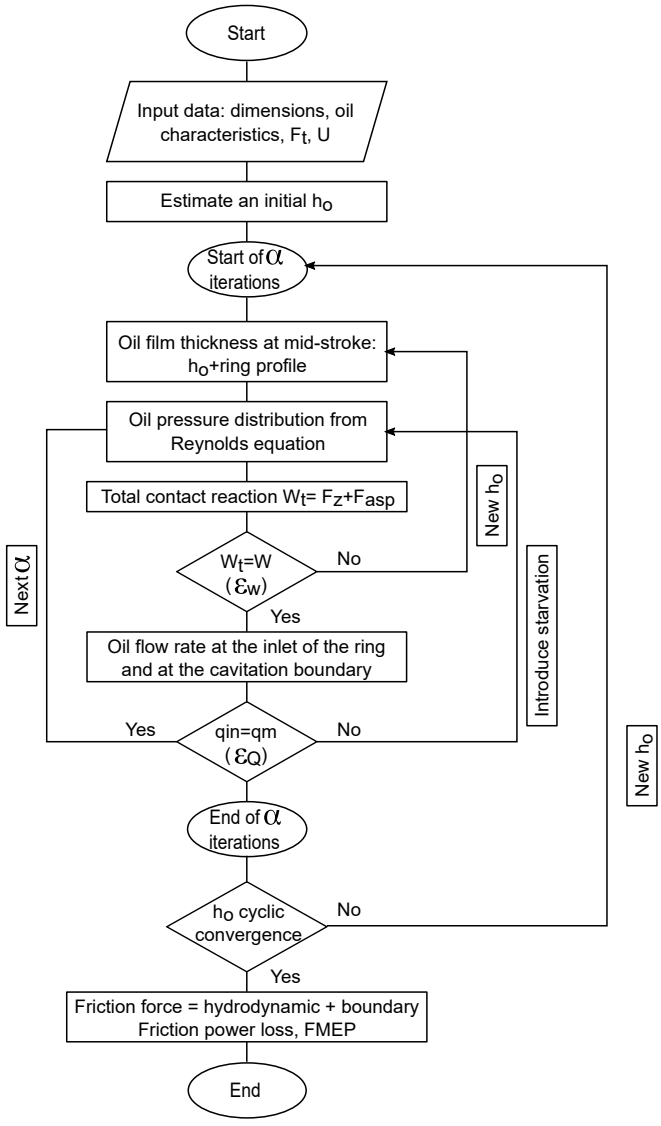

Figure 6: Flow diagram for the implementation of the piston compression ring lubrication model

An initial value of h_o was estimated in order to run the model, it was assumed to be equal to the radial clearance space between the piston and the liner internal diameter.

U is the piston speed [37]:

$$U = -R\omega\left[sin\,\alpha + \frac{R}{2L}\frac{sin2\alpha}{\sqrt{1-\left(\frac{R}{L}sin\,\alpha\right)^2}}\right] \tag{4}$$

Finally, the Reynolds equation in non-dimensional terms is as follows:

$$\frac{\partial}{\partial X}\left(H^3\frac{\partial P}{\partial X}\right) = 6\frac{\partial H}{\partial X} + 12K_t\frac{\partial H}{\partial \alpha} \tag{5}$$

To obtain the oil pressure distribution, Equation (5) was solved using the finite differences method. For the left-hand side term, and the first term in the right-hand side of the equation, a central finite difference scheme was applied; while for the squeeze term, a forward finite difference expression was employed. Equation (5) in finite differences, and solved for pressure at the node i, is as follows:

$$P_i = \frac{H^3_{i+1/2}P_{i+1} + H^3_{i-1/2}P_{i-1} - 6\delta X(H_{i+1/2} - H_{i-1/2}) - 12K_t\delta X^2\left(\frac{H_j - H_{j-1}}{\delta\alpha}\right)}{(H^3_{i+1/2} + H^3_{i-1/2})} \tag{6}$$

Once the pressure distribution was obtained for all the nodes in the ring domain at the specific crank angle, convergence was sought with the expression (7) and a tolerance ϵ_P. n represents the number of nodes on the compression ring axial profile and m is the iteration.

$$\sum_{i=1}^{n} \frac{\mid P^m_{i,j} - P^{m-1}_{i,j} \mid}{P^m_{i,j}} \leq \epsilon_P \tag{7}$$

From the oil pressure distribution, in its dimensional form p, the load carrying capacity F_z of the oil was obtained from equation (8). This force along with that from the asperities' interaction F_{asp}, should balance the ring tension force W.

$$F_z = \int_0^l p dx \tag{8}$$

To model the asperity interaction between the piston compression ring and the liner, the Greenwood and Tripp [12] model was applied to calculate the load carried by the asperities F_{asp} from equation (9). It was assumed that the asperities of both surfaces, piston ring and liner, followed a Gaussian distribution. Coefficients used in the equation are summarized in Table 5.

$$F_{asp} = \frac{16\sqrt{2}}{15}\pi(\sigma\beta\rho)^2 E\sqrt{\frac{\sigma}{\beta}}AF_{5/2}(\lambda) \tag{9}$$

A is the contact area of the ring ($A = \pi Dl$), and the statistical function $F_{5/2}$ was obtained from the expression proposed in [12], using numerical integration:

$$F_{5/2}(\lambda) = \frac{1}{\sqrt{2\pi}}\int_\lambda^\infty (s-\lambda)^{5/2} e^{-s^2/2} ds \tag{10}$$

$F_{5/2}$ is function of the Stribeck oil film parameter λ, defined as the ratio between the minimum oil film thickness h_o and the roughness of the surfaces σ. Values of λ greater than 4 indicate hydrodynamic lubrication with $F_{5/2} = 0$

The total contact reaction, $W_t = F_z + F_{asp}$, was then compared to the ring tension force W, calculated for the piston compression ring from equation (11); note that W and W_t are force per unit width.

$$W = \frac{P_c A}{b} \tag{11}$$

Where P_c is the contact pressure obtained from (12) as in reference [18, 30], and F_t is the ring tangential force Ft.

$$P_c = \frac{2F_t}{Dl} \tag{12}$$

Given that these two forces, W and W_t, applied to the ring-liner interface must be in equilibrium, they are compared for equality with the following expression (13) and tolerance ϵ_W.

$$\frac{\mid W - W_t \mid}{W} \leq \epsilon_W \tag{13}$$

If the convergence criterion was not satisfied, and iterative procedure was applied updating the minimum oil film thickness h_o using equation (14). In this way, if the total contact reaction was lower than the force applied by the ring tension, the minimum film thickness would decrease to yield a greater force and meet the convergence criterion.

$$h_{o,new} = h_{o,old} + \gamma_1 \left(\frac{W_t - W}{W} \right) \tag{14}$$

$h_{o,old}$ is the minimum film thickness obtained in the current iteration, and $h_{o,new}$ is the film thickness to be used in the following iteration. γ_1 was set between 0.02 and 0.075. Once convergence was achieved, calculation proceeded to the oil flow rate and then to the next crank angle α.

The following step was to calculate the oil flow rate per unit circumferential length from the integral of the velocity term U, which is composed by the Poiseuille and Couette terms, first and second term in the right side of equation (15), respectively:

$$q(x) = \int_0^h U(x,z)dz = \frac{-h^3}{12\eta}\frac{\partial p}{\partial x} + U\frac{h}{2} \tag{15}$$

To calculate the oil flow rate, the cavitation boundary was selected. In this way, $\partial p/\partial x = 0$, and equation (15) was reduced to the following expression (16); here h_m is the oil film thickness at the selected location.

$$q_m(x) = U\frac{h_m}{2} \tag{16}$$

Expressed in non-dimensional terms:

$$Q_m(X) = \frac{U}{U}\frac{h_m}{2h_o} = \frac{H_m}{2} \tag{17}$$

For the fully flooded lubrication condition, the last step is to achieve the cyclic convergence of the minimum oil film thickness. For this purpose, the minimum film thickness calculated in each crank angle is compared to that of the previous cycle. Convergence is achieved when the difference is less than 0.5%.

6.1. Friction force

The friction force in the interface of the piston compression ring and liner was modeled from two contributions, one due to the viscous shear of the lubricant oil, hydrodynamic lubrication, and the other determined by the asperity interaction of the surfaces, boundary lubrication.

Under hydrodynamic conditions, friction force is the result of the oil shearing in the full film and in the cavitation region (Figure 5). Due to the presence of air bubbles in the cavitation region, only a fraction of the radial clearance space between the ring and the liner is filled with oil [4]. This fraction $\hat{z}$ can be obtained from the flow continuity condition evaluated at the boundaries of the cavitation region, where the oil pressure gradient is zero:

$$\hat{z} = \frac{h_m}{h} \tag{18}$$

The viscous friction force is therefore obtained as the integral of the shear stress in the two regions:

$$f_v(x) = \int_{x_1}^{x_2} \tau dx + \int_{x_2}^{x_3} \hat{z}\tau dx \tag{19}$$

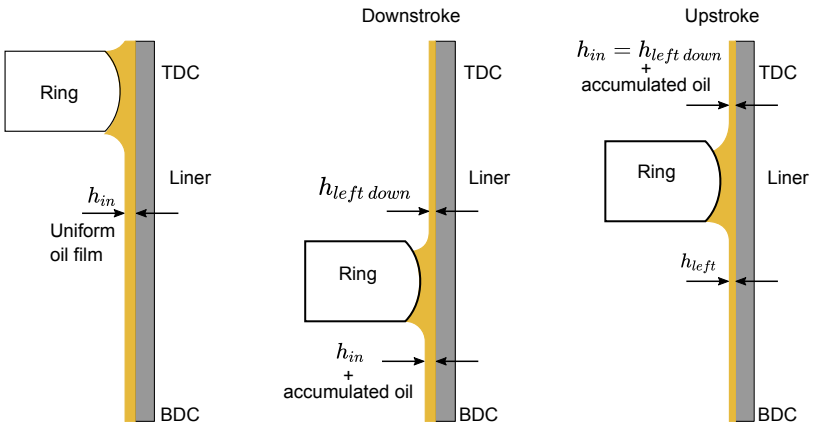

Figure 7: Oil available to the ring during the upstroke and downstroke

Where,

$$\tau = \frac{-h}{2}\frac{\partial p}{\partial x} - \eta\frac{U}{h} \tag{20}$$

The boundary friction force on the other hand, was determined from the asperity interactions with two sources: one due to the shearing of the thin oil film absorbed by the asperity peaks, first term in Equation (21). This shear has a non-newtonian behavior and is determined by the Eyring shear stress of the oil τ_o [5]. The second source is from the adhesive friction of the cold welded asperities, second term in Equation (21); where ζ is the coefficient of asperity shear strength [43].

$$f_b(x) = \tau_o A_{asp} + \zeta F_{asp} \tag{21}$$

Given that the area of asperity peaks represents a very small fraction of the total contact area of the ring, less than 0.12%, the first term of Equation (21) can be neglected [43].

Finally the total friction force f was obtained from (22):

$$f(x) = f_v(x) + f_b(x); \tag{22}$$

6.2. Ring starvation

To this part, the lubrication model assumed the inlet of the piston compression ring to be fully flooded with oil; however, given that this condition does not reflect the actual lubrication conditions of a piston compression ring in a normal engine operation, starvation was included in the model for both the up-stroke and down-stroke. The model applied by Dowson et al [3] for the piston compression ring was employed here: the oil available to the ring in the up-stroke should be equal to the oil left during the down-stroke. This oil availability condition is shown in Figure 7. In the first diagram with the piston in the TDC, the oil film at the liner h_{in} has uniform thickness; during the downstroke in the second diagram, the ring encounters this oil film thickness plus the accumulated oil and leaves behind the film thickness h_{left}. In this way, during the upstroke in the third diagram, the ring encounters the oil film thickness left at this location during the previous stroke plus the accumulated oil.

The same condition (23) applies for the whole engine cycle, where the oil available to the ring q_{in} and that left behind q_m can be calculated from equation (24) and the previous equation (16), respectively.

$$q_{in}(\text{up-stroke}) = q_m(\text{down-stroke}) \tag{23}$$

$$q_{in} = h_{in} U \tag{24}$$

Condition (23) could also be expressed and evaluated in non-dimensional terms as follows:

$$\begin{aligned} Q_{in}(\text{up-stroke}) &= Q_m(\text{down-stroke}) \\ \frac{U}{U}\frac{h_{in}}{h_o} &= \frac{U}{U}\frac{h_m}{2h_o} \\ \frac{h_{in}}{h_o} &= \frac{H_m}{2} \end{aligned} \tag{25}$$

If the ring is fully flooded at any crank angle, oil accumulation occurs at the leading edge of the ring, and it is added to the oil available in the next crank angle.

In the model described here, the flow continuity condition in Equation (23), was sought through an iterative process, as depicted in Figure 6: in the first iteration the oil inlet was set at the first node of the axial domain, the oil pressure distribution, load carrying capacity and film thickness were calculated in the same way as for the fully flooded condition. The oil flow rate entering the ring q_{in} in the up-stroke, and that left by the ring q_m in the down-stroke, were calculated and compared for equality and a tolerance ϵ_Q. If the flow continuity condition is not achieved, starvation is introduced moving the oil inlet inwards the axial domain one node at each iteration; the oil pressure distribution, load carrying capacity and film thickness calculations are repeated for the new domain. This iterative procedure is developed until convergence is achieved.

6.3. Oil rheology

As stated in Section 6, the oil viscosity was assumed to be only dependent of the temperature; furthermore, it was assumed that the viscosity of the oil entering the ring varies with the position of the ring along the stroke. For this purpose, the experimental measurements of the thermocouples installed in the liner were taken as the oil working temperature. Given that these thermocouples were located at the TDC, BDC and at the mid-stroke, a piecewise cubic hermite interpolating polynomial (PCHIP) was used to obtain the temperature along the liner for a complete engine cycle. To calculate the corresponding dynamic viscosity of the oil, the Vogel equation as stated in equation(26), was employed. a, b and c are constants of the oil, and η is the oil dynamic viscosity at the desired temperature T_0.

$$\eta = a e^{b/(T_0 - c)} \tag{26}$$

7. Results and discussion

7.1. Experimental tests

As indicated in Section 5, parameters tests in the floating liner were developed for two configurations of the piston, A and B, and four engine speed levels and three oil temperatures. Figure 8 presents the friction force measurements for some of the parameters conditions and for the piston configuration A. In order to make the results clearer, the raw friction force obtained from the sensors was filtered with a moving average filter.

From Figure 8, the lubrication regimes experienced by the piston-liner conjunction can be identified from the shape of the instantaneous friction curves: at the mid-stroke regions, hydrodynamic lubrication is promoted by the high relative motion of the surfaces and friction is determined by shearing of the oil. As the piston reduces its velocity approaching the dead centers, mixed lubrication begins to appear reflected in a small decrease of friction, followed by a rapid increase of friction at the dead centers, indicating that friction is determined by asperity contact. This boundary and mixed lubrication conditions are present until the piston speed increases and there is sufficient oil film thickness to completely separate the surfaces.

In this Figure 8, it can be observed that the working conditions of the test rig are dominated by boundary lubrication near the dead centers and specially at the lower engine speed regimes. This boundary lubrication decreases with the increase of the speed, which can be observed in the smaller peaks of friction at the dead centers for 800 and at 900 rpm. The opposite occurs with the oil temperature, its increase from 40 to 80°C results in higher friction in the dead

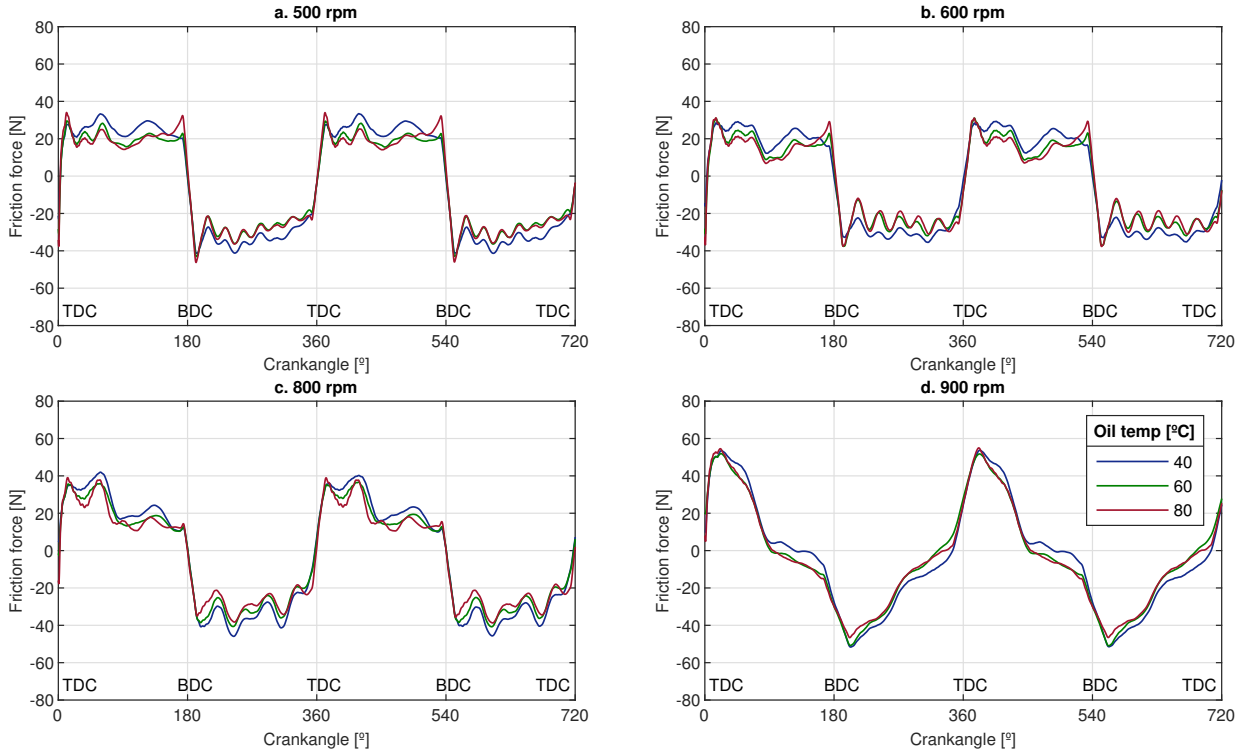

Figure 8: Friction force for the piston configuration A at different engine speed and oil temperature levels

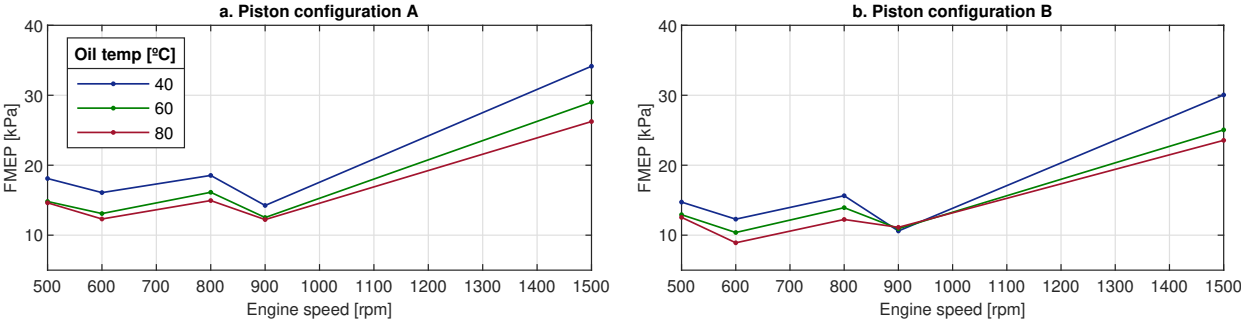

Figure 9: FMEP of the piston configurations A and B as function of the engine speed and oil temperature

centers and specially at 500 and 600 rpm, where neither the viscosity nor the engine speed contributes to the formation of a fluid film of lubricant oil. In the mid-strokes, hydrodynamic lubrication begins to appear due to the increase of the relative speed between the surfaces. In this region, a higher oil viscosity also contributes to the formation of a thicker oil film and therefore, to higher viscous friction. Under 900 rpm, it can also be observed that friction at the dead centers is not zero, as it is in the other engine speeds; instead, the friction force curve crosses zero before the dead center locations. This behavior is explained by the impact forces caused by the piston secondary motion, which are significant in this regime.

From the measured friction force curves, the FMEP was calculated for an engine cycle and plotted for the two piston configurations A and B; results are presented in Figure 9.

In Figure 9, the effect of the engine speed and oil temperature can be seen in the overall friction of an engine cycle. With the increase of the engine speed, the prevalence of hydrodynamic lubrication results in an increase of the viscous friction and therefore on the FMEP. The opposite can be said for 500 rpm, where the FMEP increases due to the major contribution of boundary/mixed friction near the dead centers. Regarding the oil temperature, comparison of results

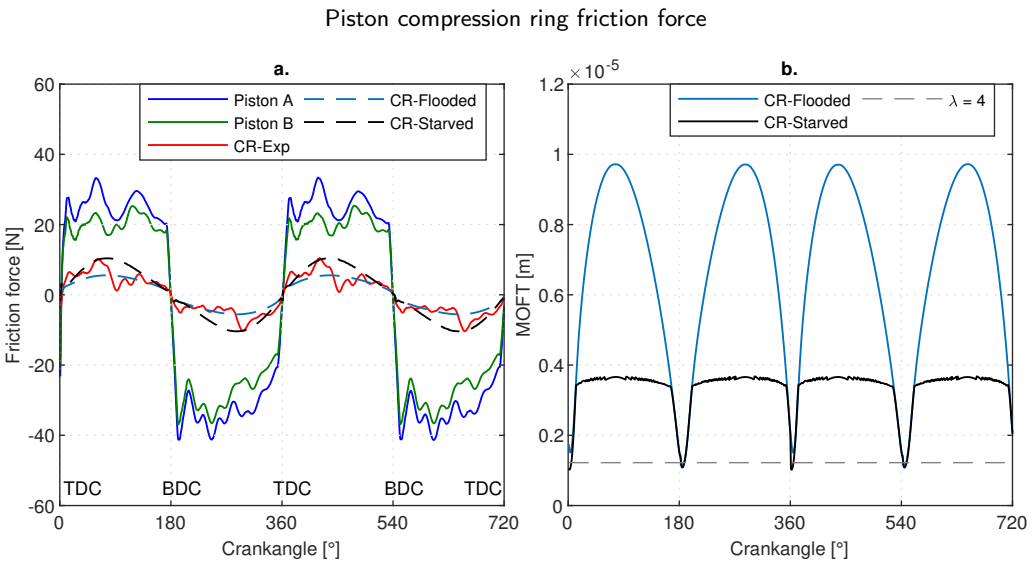

Figure 10: Experimental and theoretical results of the compression ring friction force at 500 rpm and 40° C

at 60 and 80°C shows small differences in FMEP; this is due to the viscosity characteristics of the oil formulation: the viscosity step between 40 and 60°C is greater than that for 60 and 80°C, as presented in Table 5. This trend appeared for most of the speed regimes. At 500 rpm, the FMEP values for 60 and 80°C are almost the same for both piston configurations A and B, with only a small difference in the friction force measurement at the BDC (Figure 8a.) At 900 rpm on the other hand, the piston secondary motion begins to interfere with the friction force measurements, causing impact forces due to the inertia of the system. This effect is more evident in the piston configuration B, where the absence of the compression ring results in a larger radial clearance between the piston and the liner. Under this engine speed, the FMEP results in Figure 9b. were practically the same for the three oil temperature levels. As commented previously, this situation shows that the effect of the piston secondary motion at this regime is significant, masking the actual effect of the oil temperature/viscosity over the friction losses variation in the piston-liner interface.

7.2. Compression ring friction force: comparison of experimental and theoretical results

This section presents the comparison of results for the piston compression ring between the experimental measurements and the friction force estimations obtained from the lubrication model described in Section 6. As explained in Section 5, the experimental friction force share of the compression ring was obtained from the subtraction of the measurements of the piston configurations A and B. Regarding the theoretical estimations, friction force is presented for the two lubrication conditions: first, assuming that the ring is flooded with oil throughout the engine cycle and second, including lubricant starvation.

Figures 10a, 11a and 12a, gather the experimental friction force measurements for the piston configuration A and B, and the resultant friction force of the compression ring for some representative test points: 500 rpm and 40°C, 600 rpm and 60°C, and 800 rpm and 80°C, respectively. The contribution of the compression ring to the total friction force of the piston is highly significant for the configuration and working conditions of the floating liner, reflected in the space formed between the measurements of piston A and B. Furthermore, it can be seen that the compression ring contribution is present throughout the engine cycle and therefore, in all the lubrication regimes. At 600 rpm and 60°C (Figure 11a) however, the friction share of the compression ring decreases to almost zero contribution at the BDC, possibly due to the supply of oil from the crankcase being enough to fill the compression ring inlet during the downstroke; at the BDC reversal however, the friction share of the compression ring appears again.

These previous figures also include the predicted friction force for the piston compression ring for fully flooded and starved lubrication conditions. The minimum oil film thickness (MOFT) was also included in Figures 10b, 11b and 12b for the two lubrication regimes. The dotted line in the figures shows the Stribeck oil film parameter λ, defined as the limit for hydrodynamic lubrication.

From the MOFT results, it can be observed that the assumption of ring starvation, which reduces the wetted area of the ring, significantly affects the thickness of the oil film at the mid-strokes. This is due to the high oil pressures

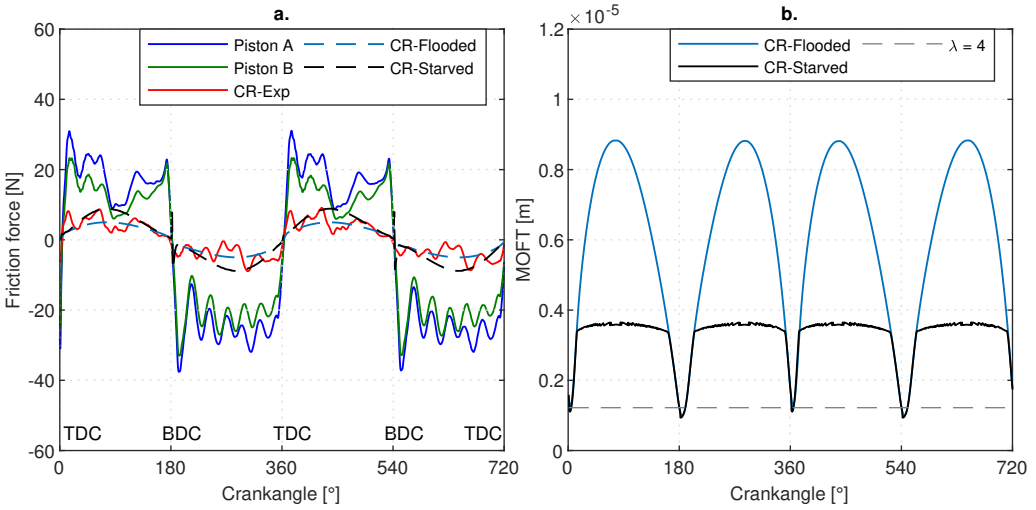

Figure 11: Experimental and theoretical results of the compression ring friction force at 600 rpm and 60° C

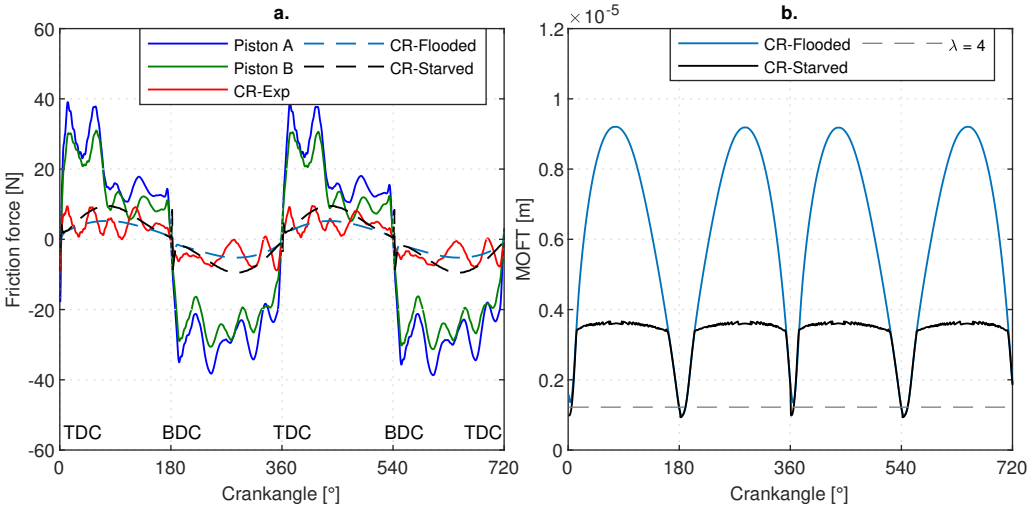

Figure 12: Experimental and theoretical results of the compression ring friction force at 800 rpm and 80° C

needed to produce the oil carrying capacity to balance the applied load. In this way, the reduction of the film thickness results in higher friction forces, according to the relationship for the viscous shear stress and the oil film ($\tau \propto \eta U/h$). Near the dead centers, the reduction of the relative speed results in greater oil pressures to overcome the applied load, and therefore in lower MOFTs. In these regions, the contribution of the pressure gradient to the viscous friction becomes more prominent, first term in equation (20). Due to the characteristics of the compression ring and its working conditions, most of the engine cycle presents hydrodynamic lubrication with just a few crank angles dominated by the asperity interactions.

Overall, the friction force estimation from the fully flooded lubrication model shows good agreement with the experimental measurements, both in terms of the curve trends and the magnitude of the friction force. For the starved lubrication model on the other hand, results show that the friction force is slightly overestimated at the lower engine speed regimes, but increases significantly with the engine speed as shown in Figure 13. This figure presents the results of the rest of the test points in terms of FMEP, obtained for a complete engine cycle of 720°, with the aim of making a clearer comparison between the experimental and theoretical results. The standard deviation (STD) of the experimental measurements for the compression ring was also plotted in this figure; as it can be seen the deviation was small with

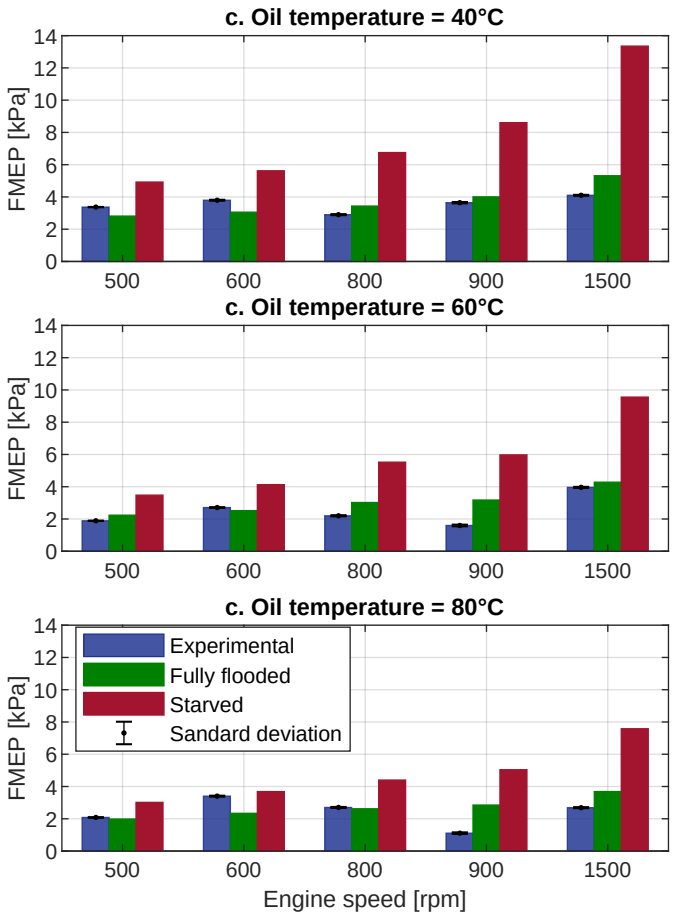

Figure 13: Experimental and theoretical FMEP results for the piston compression ring

a maximum relative STD of 1.54% (STD=49.1 Pa at 900 rpm, 80°C) and a minimum of 0.35% (STD=11.8 Pa at 500 rpm, 40°C).

From this Figure 13, it can be seen that the experimental FMEP and the that of the fully flooded lubrication model are in good agreement for most of the test conditions. At 900 rpm however, it is important to note that the results of the experimental tests with the piston configuration B showed a poor response due to vibrations in the test rig aggravated by the increased clearance between the piston and the liner, as shown in Figure 9b., where it can be seen that the FMEP fell to almost the same value for all the oil temperature levels. This condition leads to an incorrect comparison with the model estimations.

Regarding the FMEP comparison with the starved lubrication model, as explained in Section 6.2 and shown in Figure 7, the oil available to the compression ring is taken from the oil left by itself during the previous stroke, it means, that during the downstroke, the oil supplied from the crankcase and the oil jets is not taken into account. In the experimental tests, and taking into account that the floating liner is motored under ambient pressure conditions, it is possible that in the downstroke, the compression ring has a sufficient amount of oil, as seems to be the case at 600 rpm and 60°C (Figure 11). This could be one of the reasons for the differences in FMEP between the experimental results and the starved model. The inclusion of the scraper ring and the oil control ring to the model, would give a better estimation of the oil available to the rings at each crank angle, and therefore of the lubrication conditions that they experience.

8. Conclusions

- The floating liner test rig showed to provide instantaneous friction force measurements of the piston-cylinder liner assembly with an appropriate response to the changes in the working conditions of the rig, engine speed and oil temperature. Furthermore the configuration of the floating liner allowed the development of multiple parameters tests with repetitive and reproducible results. These parameters test also showed that above 800 rpm, vibration and specially the piston secondary motion start to interfere with the friction measurements. Improvements to the test rig structure are needed to obtain a cleaner measurement at higher speed regimes.
- The experimental results with the piston configuration A and B showed that the contribution of the piston compression ring to the total friction force is significant throughout the engine cycle: during the boundary/mixed lubrication regime at the dead centers due to its tension force and the low engine speed, and during hydrodynamic lubrication at the mid-strokes due to the wedge effect caused by its running profile.
- The experimental friction force curves showed that, although it is possible to obtain reasonable measures of the compression ring friction force with the subtraction method used in this study, the clearance between the piston and the liner without this ring results in high instability of the measurements. This issue could be solved using a slightly over-sized piston.
- Results obtained with the floating liner under different working conditions helped to validate the piston compression ring lubrication model. Assuming fully flooded lubrication, the comparison of results showed good agreement between the experimental and theoretical results. For the starved lubrication approach, a better estimation of the degree of starvation is needed to better simulate the lubrication of the ring. This could be addressed with the analysis of the oil available to the rings from the interaction of the complete piston ring pack.

Acknowledgments

Author Sophia Bastidas would like to thank to the support of the program Ayudas de Investigación y Desarrollo (PAID-01-17) of the Universitat Politècnica de València.

CRediT authorship contribution statement

Vicente Macián: Supervision, Conceptualization. **Bernardo Tormos:** Validation, Writing - Review and Editing. **Vicente Bermúdez:** Resources, Methodology. **Sophia Bastidas:** Investigation, Software, Formal analysis, Writing - Original Draft.

References

[1] D'Agostino, V., della Valle, S., Ruggiero, A., Senatore, A., 2002. A study on the piston top ring lubrication using the open-end boundary condition, in: Aimeta International Tribology Conference, Italy.

[2] Delprete, C., Razavykia, A., Baldissera, P., 2019. Detailed analysis of piston secondary motion and tribological performance. International Journal of Engine Research 0, 1468087419833883. doi:10.1177/1468087419833883.

[3] Dowson, D., Economou, P.N., Ruddy, B.L., Strachan, P.J., Baker, A.J.S., 1979. Piston ring lubrication. Part II. Theoretical analysis of a single ring and a complete ring pack. Energy conservation through fluid film lubrication technology: frontiers in research and design , 23–52.

[4] Dowson, D., Higginson, G.R., Archard, J.F., Crook, A.W., 1977. Elasto-hydrodynamic lubrication: international series on materials science and technology. Pergamon Press.

[5] Eyring, H., 1936. Viscosity, plasticity, and diffusion as examples of absolute reaction rates. The Journal of chemical physics 4, 283–291.

[6] Ezhilmaran, V., Vasa, N., Vijayaraghavan, L., 2018. Investigation on generation of laser assisted dimples on piston ring surface and influence of dimple parameters on friction. Surface and Coatings Technology 335, 314–326. doi:10.1016/J.SURFCOAT.2017.12.052.

[7] Furuhama, S., Sasaki, S., 1983. New device for the measurement of piston frictional forces in small engines, in: 1983 SAE International Off-Highway and Powerplant Congress and Exposition, SAE International. doi:10.4271/831284.

[8] Furuhama, S., Takiguchi, M., 1980. Measurement of piston frictional force in actual operating diesel engine. SAE Technical Paper Series 1, 2896–2914. doi:10.4271/790855.

[9] Gore, M., Rahmani, R., Rahnejat, H., King, P., 2016. Assessment of friction from compression ring conjunction of a high-performance internal combustion engine: A combined numerical and experimental study. Proceedings of the Institution of Mechanical Engineers, Part C: Journal of Mechanical Engineering Science 230, 2073–2085. doi:10.1177/0954406215588480.

[10] Gore, M., Theaker, M., Howell-Smith, S., Rahnejat, H., King, P.D., 2014. Direct measurement of piston friction of internal-combustion engines using the floating-liner principle. Proceedings of the Institution of Mechanical Engineers, Part D: Journal of Automobile Engineering 228, 344–354. doi:10.1177/0954407013511795.

[11] Grabon, W., Pawlus, P., Wos, S., Koszela, W., Wieczorowski, M., 2017. Effects of honed cylinder liner surface texture on tribological properties of piston ring-liner assembly in short time tests. Tribology International 113, 137–148. doi:10.1016/J.TRIBOINT.2016.11.025.
[12] Greenwood, J.A., Tripp, J.H., 1970. The contact of two nominally flat rough surfaces. Proceedings of the Institution of Mechanical Engineers 185, 625–633. doi:10.1243/PIME_PROC_1970_185_069_02.
[13] Ha, G.P., Kim, J.S., Jo, M.R., O, D.Y., 2002. Development of piston friction force measurement system. Transactions of the Korean Society of Mechanical Engineers A 26, 1608–1614. doi:10.3795/KSME-A.2002.26.8.1608.
[14] Higuchi, T., Mabuchi, Y., Ichihara, H., Murata, T., Moronuki, M., 2017. Development of hydrogen-free diamond-like carbon coating for piston rings. Tribology Online 12, 117–122. doi:10.2474/trol.12.117.
[15] Holmberg, K., Andersson, P., Nylund, N., Mäkelä, K., Erdemir, A., 2014. Global energy consumption due to friction in trucks and buses. Tribology International 78, 94–114. doi:10.1016/J.TRIBOINT.2014.05.004.
[16] Islam, M.R., 2016. A floating liner facility and studies of friction at a reciprocating piston-cylinder wall interface. Doctoral Thesis. University of Nottingham.
[17] James, C.J., 2012. Analysis of Parasitic Losses in Heavy Duty Diesel Engines. Doctoral Thesis. Massachusetts Institute of Technology.
[18] Jeng, Y., 1992. Theoretical analysis of piston-ring lubrication part 1 fully flooded lubrication. Tribology Transactions 35, 696–706. doi:10.1080/10402009208982174.
[19] Kikuchi, T., Ito, S., Nakayama, Y., 2003. Piston friction analysis using a direct-injection single-cylinder gasoline engine. JSAE review 24, 53–58. doi:10.1016/S0389-4304(02)00242-4.
[20] Kim, K., Godward, T., Takiguchi, M., Aoki, S., 2007. Part 2: The effects of lubricating oil film thickness distribution on gasoline engine piston friction, in: SAE World Congress & Exhibition, SAE International. doi:10.4271/2007-01-1247.
[21] Kunkel, S., Werner, M., Wachtmeister, G., 2011. Setting up a measuring device to determine the friction of the piston assembly. SAE International Journal of Materials and Manufacturing 4, 340–351. doi:10.4271/2011-01-0227.
[22] Law, T., MacMillan, D., Shayler, P.J., Kirk, G., Pegg, I., Stark, R., 2012. A new floating-liner test rig design to investigate factors influencing piston-liner friction, in: SAE 2012 World Congress and Exhibition, SAE International. doi:10.4271/2012-01-1328.
[23] Liao, K., Liu, Y., Kim, D., Urzua, P., Tian, T., 2012. Practical challenges in determining piston ring friction. Proceedings of the Institution of Mechanical Engineers, Part J: Journal of Engineering Tribology 227, 112–125. doi:10.1177/1350650112465364.
[24] Liu, Y., Kim, D., Westerfield, Z., Meng, Z., Tian, T., 2018. A comprehensive study of the effects of honing patterns on twin-land oil control rings friction using both a numerical model and a floating liner engine. Proceedings of the Institution of Mechanical Engineers, Part J: Journal of Engineering Tribology 233, 1–27. doi:10.1177/1350650118774395.
[25] Ma, M.T., Sherrington, I., Smith, E.H., 1996. Implementation of an algorithm to model the starved lubrication of a piston ring in distorted bores: Prediction of oil flow and onset of gas blow-by. Proceedings of the Institution of Mechanical Engineers, Part J: Journal of Engineering Tribology 210, 29–44. doi:10.1243/PIME_PROC_1996_210_475_02.
[26] Ma, M.T., Sherrington, I., Smith, E.H., 1997. Analysis of lubrication and friction for a complete piston-ring pack with an improved oil availability model: Part 1: Circumferentially uniform film. Proceedings of the Institution of Mechanical Engineers, Part J: Journal of Engineering Tribology 211, 1–15. doi:10.1243/1350650971542273.
[27] Madden, D., Kim, K., Takiguchi, M., 2006. Part 1: Piston friction and noise study of three different piston architectures for an automotive gasoline engine, in: SAE 2006 World Congress & Exhibition, SAE International. doi:10.4271/2006-01-0427.
[28] Moore, S.L., Hamilton, G.M., 1978. The starved lubrication of piston rings in a diesel engine. Journal of Mechanical Engineering Science 20, 345–352. doi:10.1243/JMES_JOUR_1978_020_060_02.
[29] Morris, N., Rahmani, R., Rahnejat, H., King, P.D., Fitzsimons, B., 2013. The influence of piston ring geometry and topography on friction. Proceedings of the Institution of Mechanical Engineers, Part J: Journal of Engineering Tribology 227, 141–153. doi:10.1177/1350650112463534.
[30] Okamoto, M., Sakai, I., 2001. Contact pressure distribution of piston rings -calculation based on piston ring contour-, in: SAE 2001 World Congress, SAE International. doi:10.4271/2001-01-0571.
[31] O'Rourke, B., Radford, D., Stanglmaier, R., 2010. Tri-axial force measurements on the cylinder of a motored SI engine operated on lubricants of differing viscosity. Journal of Engineering for Gas Turbines and Power 132, 092807. doi:10.1115/1.4000608.
[32] O'Rourke, B., Stanglmaier, R., Radford, D., 2006. Development of a floating-liner engine for improving the mechanical efficiency of high performance engines, in: Motorsports Engineering Conference & Exposition, SAE International. doi:10.4271/2006-01-3636.
[33] Overgaard, H., Klit, P., Vølund, A., 2018. Investigation of different piston ring curvatures on lubricant transport along cylinder liner in large two-stroke marine diesel engines. Proceedings of the Institution of Mechanical Engineers, Part J: Journal of Engineering Tribology 232, 85–93. doi:10.1177/1350650117744100.
[34] Patir, N., S Cheng, H., 1978. An average flow model for determining effects of three-dimensional roughness on partial hydrodynamic lubrication. Journal of Tribology 100, 12–17. doi:10.1115/1.3453103.
[35] Priest, M., Dowson, D., Taylor, C.M., 2000. Theoretical modelling of cavitation in piston ring lubrication. Proceedings of the Institution of Mechanical Engineers, Part C: Journal of Mechanical Engineering Science 214, 435–447. doi:10.1243/0954406001523092.
[36] Profito, F.J., Vlădescu, S.C., Reddyhoff, T., Dini, D., 2017. Transient experimental and modelling studies of laser-textured micro-grooved surfaces with a focus on piston-ring cylinder liner contacts. Tribology International 113, 125–136. doi:10.1016/J.TRIBOINT.2016.12.003.
[37] Rahnejat, H., 2010. Tribology and dynamics of engine and powertrain: fundamentals, applications and future trends. Elsevier.
[38] Richardson, D.E., 2000. Review of power cylinder friction for diesel engines. Journal of Engineering for Gas Turbines and Power 122, 506–519. doi:10.1115/1.1290592.
[39] Söderfjäll, M., Almqvist, A., Larsson, R., 2016. Component test for simulation of piston ring-cylinder liner friction at realistic speeds. Tribology International 104, 57–63. doi:10.1016/j.triboint.2016.08.021.
[40] Söderfjäll, M., Herbst, H.M., Larsson, R., Almqvist, A., 2017. Influence on friction from piston ring design, cylinder liner roughness and

lubricant properties. Tribology International 116, 272–284. doi:10.1016/J.TRIBOINT.2017.07.015.

[41] Sui, P.C., Ariga, S., 1993. Piston ring pack friction and lubrication analysis of an automotive engine using a mixed lubrication model, in: International Pacific Conference On Automotive Engineering, SAE International. doi:10.4271/931937.

[42] Taylor, C.M., 1993. Engine tribology. volume 26. Elsevier.

[43] Teodorescu, M., Taraza, D., Henein, N.A., Bryzik, W., 2003. Simplified elasto-hydrodynamic friction model of the cam-tappet contact, in: SAE 2003 World Congress & Exhibition, SAE International. doi:10.4271/2003-01-0985.

[44] Vlădescu, S., Ciniero, A., Tufail, K., Gangopadhyay, A., Reddyhoff, T., 2017. Looking into a laser textured piston ring-liner contact. Tribology International 115, 140–153. doi:10.1016/J.TRIBOINT.2017.04.051.

[45] Wakuri, Y., Hamatake, T., Soejima, M., Kitahara, T., 1992. Piston ring friction in internal combustion engines. Tribology International 25, 299 – 308. doi:10.1016/0301-679X(92)90027-K.

[46] Wakuri, Y., Soejima, M., Kitahara, T., Nunotani, M., Kabe, Y., 1995. Characteristics of piston ring friction: influences of lubricating oil properties. JSME international journal 38, 593–600. doi:10.1299/jsmec1993.38.593.

[47] Westerfield, Z., Liu, Y., Kim, D., Tian, T., 2016a. A study of the friction of oil control rings using the floating liner engine. SAE International Journal of Engines 9, 1807–1824. doi:10.4271/2016-01-1048.

[48] Westerfield, Z., Totaro, P., Kim, D., Tian, T., 2016b. An experimental study of piston skirt roughness and profiles on piston friction using the floating liner engine, in: SAE 2016 World Congress & Exhibition, SAE International. doi:10.4271/2016-01-1043.

[49] Zavos, A., Nikolakopoulos, P.G., 2018. Tribology of new thin compression ring of fired engine under controlled conditions-a combined experimental and numerical study. Tribology International 128, 214–230. doi:10.1016/J.TRIBOINT.2018.07.034.